Supplement of

Interannual variability of the winter sea ice edge in the Southern Ocean tuned by topography and oceanic transport.

Hugues Goosse[1], Cecile Davrinche[1], Benjamin Richaud[1], Dániel Topál[1], Stephy Libera[1], Alberto C. Naveira Garabato[2], Alessandro Silvano[2], Martin Vancoppenolle[3] , Pablo Ortega[4]

[1]Earth and Life Institute, Université catholique de Louvain, Louvain-la-Neuve, Belgium
[2]Ocean and Earth Science, National Oceanography Centre, University of Southampton, Southampton, UK.
[3]Sorbonne Université, Laboratoire d'Océanographie et du Climat (LOCEAN-IPSL), CNRS/IRD/MNHN, Paris, France
[4]Barcelona Supercomputing Center, Barcelona, Spain.

Correspondence to H. Goosse (hugues.goosse@uclouvain.be)

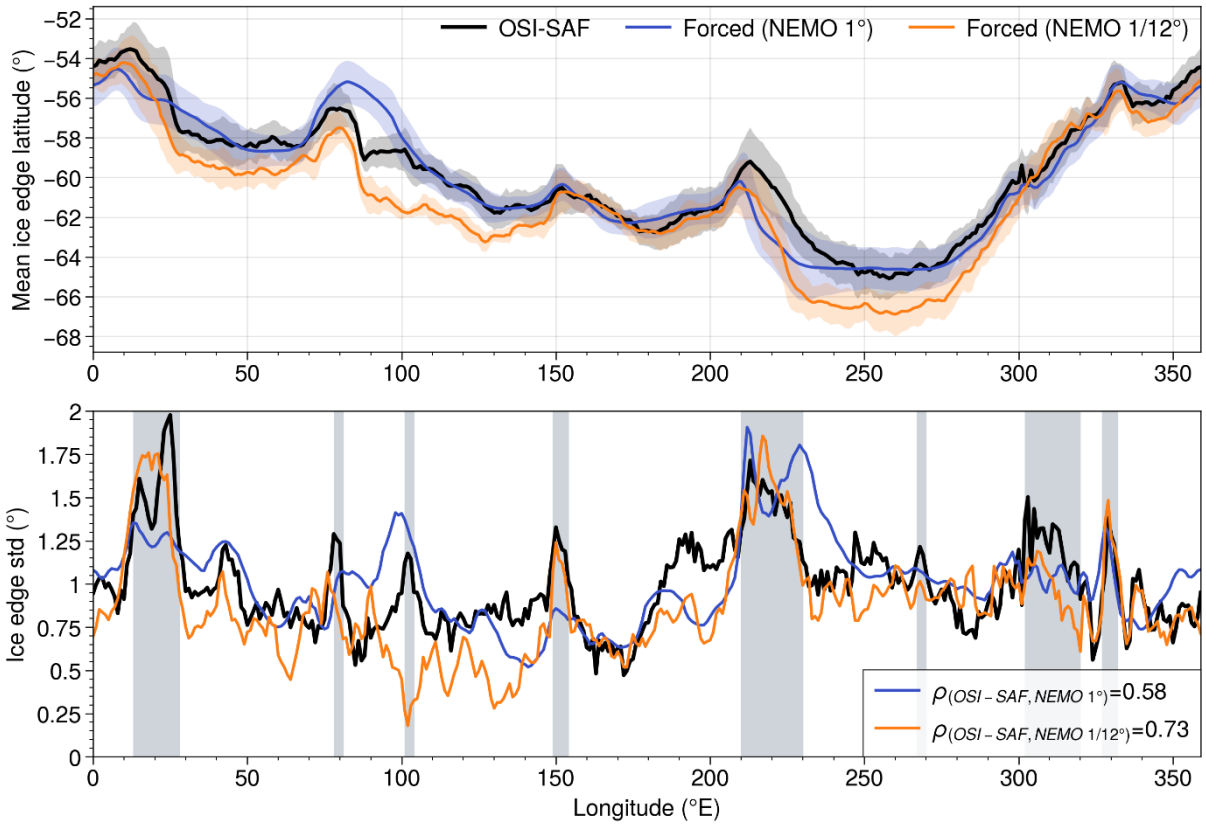

Figure S1. Mean position (top) and standard deviation of the winter ice edge (bottom) in observations (in °, black) and in NEMO-ERA5 over the period 1985-2024 at two resolutions : 1/12° (orange) and in 1° (blue).

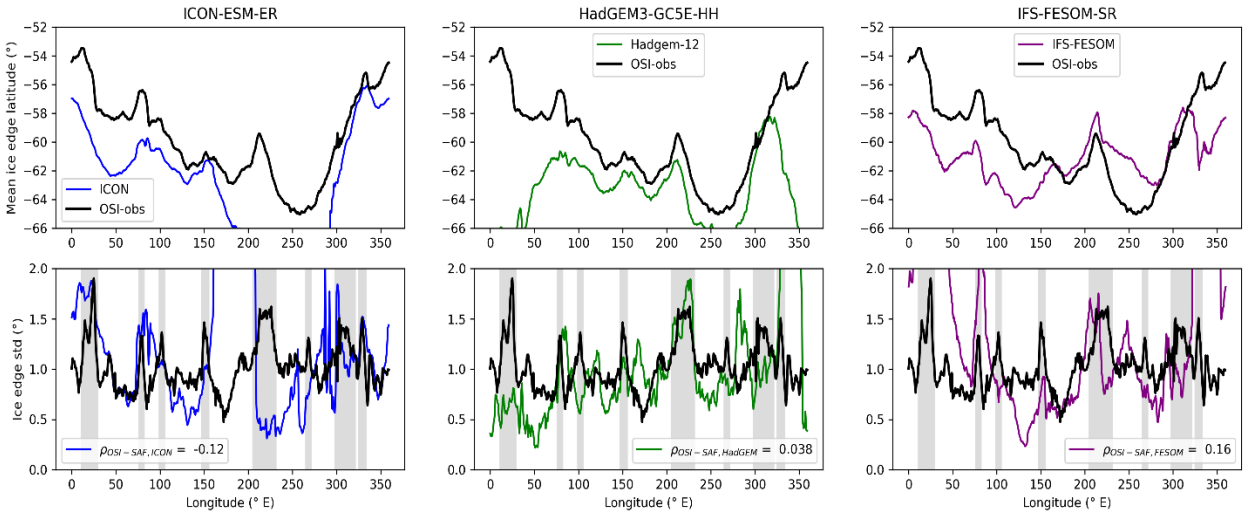

Figure S2. Top raw: Mean position of the winter ice edge in observations (in °, black) and in three high resolution coupled climate models. Bottom raw: standard deviation of the winter ice edge position (in °) in observations and for the same models. The period 1979-2025 is used for the observations and the last 30 years of the historical runs for the coupled model. Results are shown for the ICON-ESM-ER (blue), HadGEM3-GS5-HH (green) and IFS-FESOM-SR (magenta) models. The models all have an oceanic resolution of the order of 10 km globally, similar to the one of IFS-NEMO. Their oceanic, atmospheric and sea ice components are listed in Table S1. ICON-ESM-ER and IFS-FESOM-SR use FESIM as their sea ice component while HadGEM3-GS5-HH uses SI^3. These three models are characterized by regions of very high variability of the ice edge position, with values that are out of the plotted ranges, that are associated with the opening of open ocean polynyas. This large local variability leads to an overestimation of the standard deviation of the sea ice extent in winter with values of 0.7 10^6 km^2, 0.8 10^6 km^2, 1.9 10^6 km^2, in HadGEM3-GS5-HH, ICON-ESM-ER and IFS-FESOM-SR respectively, compared to an observed estimate for the period 1979-2025 of 0.5 10^6 km^2. In regions where models strongly underestimate the ice cover, like between 180 and 300°E in ICON-ESM-ER or between 0 and 50°E in HadGEM3-GC5-HH, the standard deviation of the ice edge position is also much lower than the observed one. By contrast, some of the observed peaks in the standard deviation of the ice edge position are well simulated close to the main bathymetric elements at 90°E and 220°E for instance.

a)

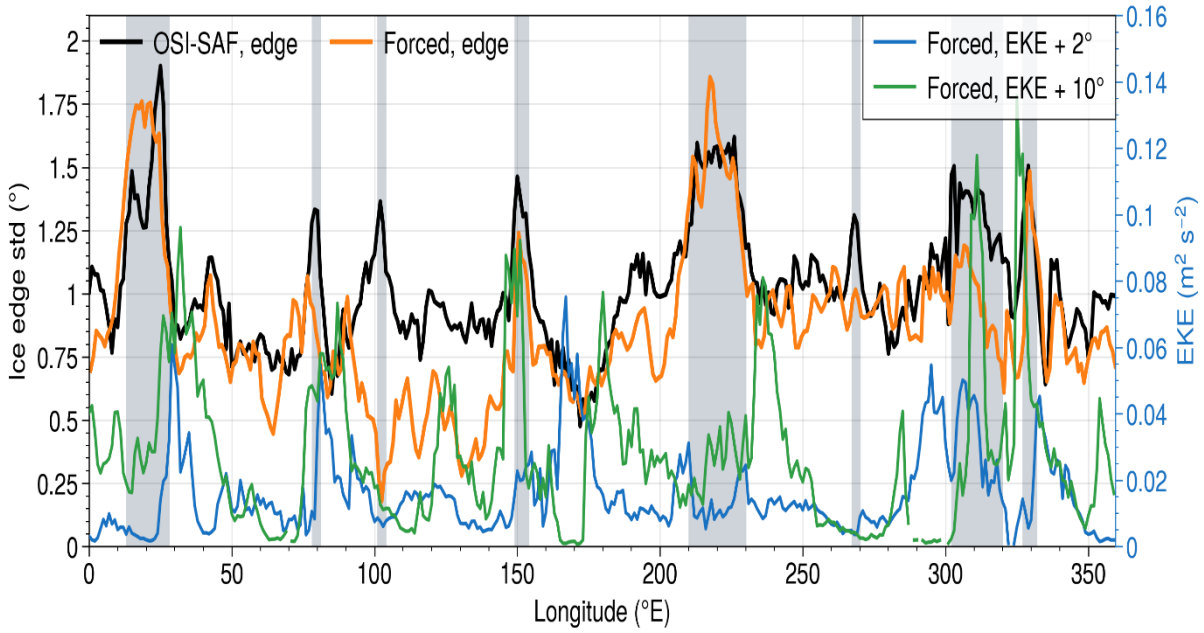

b)

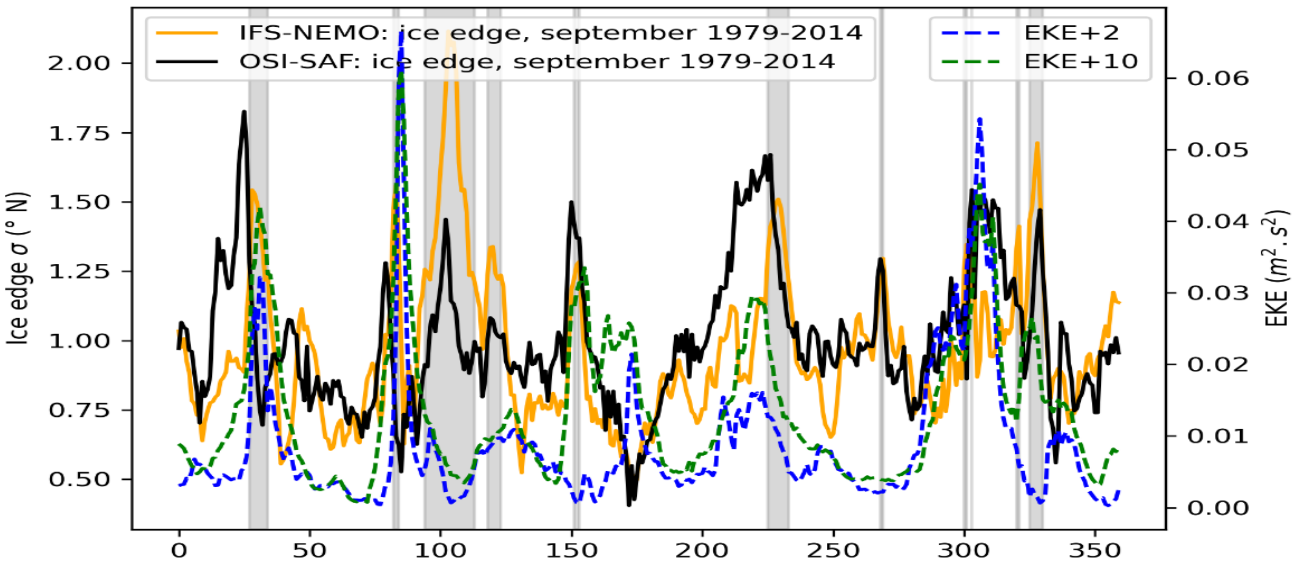

Figure S3. a) Standard deviation of the winter ice edge position for the period 1995-2024 (in °, black) and mean Eddy Kinetic Energy (EKE, m^2s^{-2}) averaged in the region 10° northward of the mean ice edge (m^2s^{-2}, in green) and in the region 2° northward of the mean ice edge (m^2s^{-2}, in blue) in NEMO driven by ERA5. b) Same as a) for IFS-NEMO over the period 1979-2014. The link between the EKE and the standard deviation of the winter ice edge position is clear in both models but is stronger in IFS-NEMO, likely because this is a self-consistent data set while part of the variability is directly imposed by the forcing in NEMO driven by ERA5.

Table S1: General characteristics of EERIE models' components

Model name	**ICON**	**IFS-FESOM**	**HadGEM3-GC5-EERIE**	**IFS-NEMO**
Ocean model	ICON-O v2.6.6	FESOM 2.5	NEMO v4.0.4	NEMO v4.0.7
Atmosphere model	ICON-A	IFS CY48R1	UM (Met Office Unified Model)	IFS CY48R1
Sea ice model	FESIM	FESIM	SI^3	SI^3
Horizontal resolution of the ocean model	Unstructured icosahedral grid. 5 km resolution globally.	Unstructured grid, ~13 km at the equator, ~5.5 km at 60°	Tripolar grid, 1/12°. 9.2 km at the equator, 4.6 km at 60°	Tripolar grid, 1/12°. 9.2 km at the equator, 4.6 km at 60°
Number of vertical levels in the ocean model	72	70	75	75
Reference	Hohenegger et al., 2023	Ghosh et al., 2026	Roberts et al., 2024	Madec et al., 2019, Vancoppenolle et al., 2023

Supplementary discussion.

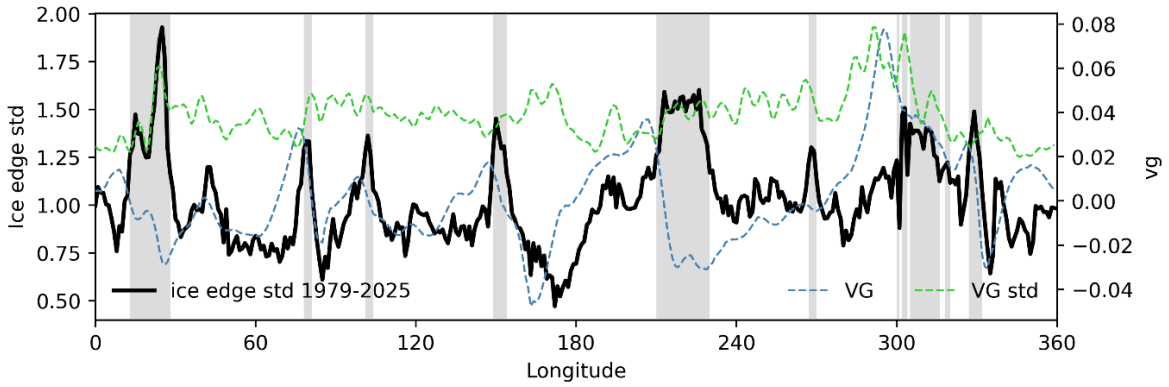

Figure S4. Standard deviation of the winter ice edge position (in °, black) and mean meridional geostrophic velocity derived from monthly mean sea surface elevation (Dragomir 2024) averaged over the region 5° northward and 5° southward of the mean ice edge (m s^{-1}, in dotted blue) and standard deviation of the mean meridional geostrophic velocity averaged over the region 5° northward and 5° southward of the mean ice edge (m s^{-1}, in dotted green). The grey zones represent the longitude bands for which the standard deviation of the ice edge is larger than 1.2° for the period 1979-2025.

The correlation between the standard deviation of the ice edge position and the mean meridional geostrophic velocity is low, with a value of 0.13 (Fig. S4). Nevertheless, a local maximum of the mean meridional geostrophic velocity is present a few degrees to the west of all the peaks in the standard deviation of the ice edge position. If we apply a shift of 13° to the east on the geostrophic velocity, the correlation with the standard deviation of the ice edge position reaches 0.46 (corresponding to the maximum lagged correlation for any longitudinal shift). This relatively high correlation is intriguing as there is no clear and established mechanism that would explain why a northward oceanic velocity would be associated with more variability of the ice edge a few degrees eastward and why southward current, which are bringing heat from the north, would have a much weaker influence. One possibility would be that those northward oceanic currents contribute more to the sea ice transport, potentially leading to more variability at the ice edge, than southward current, originating from warmer, potentially ice-free regions. However, neither the sea ice velocity nor its variance display peaks westward of the maxima in the standard deviation of the ice edge (Fig. 5)

Another explanation of this asymmetry between the role of northward and southward currents could be the transport of colder water masses originating from the south that would favor a larger response of the sea ice to the atmospheric variability. This would be consistent with Spira et al. (2024) who show an export of Winter Water (the water close to the freezing point located just below the mixed layer in summer) mainly in the regions of northward meridional currents (see for instance their Fig. 10). Specifically, the presence of colder Winter Water or of a colder pycnocline could reduce the magnitude of the negative feedback (Martinson 1990) that stabilizes the sea ice cover, leading to a larger variability compared to regions under the influence of warmer water at depth originating from the north.

Nevertheless, those two explanations are highly speculative at this stage and do not provide a clear justification for the about 10° shift between the meridional northward current and the high variability

of the ice edge position. A more likely origin of the high correlation could be found on the influence of the topography on both the mean currents and the EKE. When the currents of the Southern Ocean encounter a topographic obstacle, they tend to be diverted northward (Rintoul, 2001; Patmore et al., 2019; Jouanno and Capet, 2020) while EKE hotspots are present eastward of those topographic obstacles. This induces a shift of a few degrees between local maxima in meridional currents and EKE. As EKE has a large influence of the ice edge variability as discussed in the main text, this could explain the high correlation between the standard deviation of the ice edge position and the mean geostrophic velocity when a shift of about 10° is applied.

Supplementary references

Ghosh, R., Cheedela, S. K., Beyer, S., Koldunov, N., Berzina, S., Delpech, A., Loza, S., Wikramage, C., Libera, S., Aengenheyster, M., John, A., Remedio, A. , Scholz, P., Sidorenko, D., Streffing, J., Wachsmann, F., and Jung, T: Century-long kilometre-scale Ocean eddy-rich global climate simulation with the coupled IFS-FESOM model, submitted to Geoscientific Model Development, 2026

Hohenegger, C., Korn, P., Linardakis, L., Redler, R., Schnur, R., Adamidis, P., Bao, J., Bastin, S., Behravesh, M., Bergemann, M., Biercamp, J., Bockelmann, H., Brokopf, R., Brüggemann, N., Casaroli, L., Chegini, F., Datseris, G., Esch, M., George, G., Giorgetta, M., Gutjahr, O., Haak, H., Hanke, M., Ilyina, T., Jahns, T., Jungclaus, J., Kern, M., Klocke, D., Kluft, L., Kölling, T., Kornblueh, L., Kosukhin, S., Kroll, C., Lee, J., Mauritsen, T., Mehlmann, C., Mieslinger, T., Naumann, A. K., Paccini, L., Peinado, A., Praturi, D. S., Putrasahan, D., Rast, S., Riddick, T., Roeber, N., Schmidt, H., Schulzweida, U., Schütte, F., Segura, H., Shevchenko, R., Singh, V., Specht, M., Stephan, C. C., von Storch, J.-S., Vogel, R., Wengel, C., Winkler, M., Ziemen, F., Marotzke, J., and Stevens, B.: ICON-Sapphire: simulating the components of the Earth system and their interactions at kilometer and subkilometer scales. Geoscientific Model Development 16, 779–811, https://doi.org/10.5194/gmd-16-779-2023, 2023.

Jouanno, J., and Capet, X.: Connecting flow–topography interactions, vorticity balance, baroclinic instability and transport in the Southern Ocean: the case of an idealized storm track, Ocean Sci., 16, 1207–1223, https://doi.org/10.5194/os-16-1207-2020, 2020.

Patmore, R. D., Holland, P. R., Munday, D. R., Naveira Garabato, A. C., Stevens, D. P., and Meredith, M. P.: Topographic control of Southern Ocean gyres and the Antarctic Circumpolar Current: A barotropic perspective, J. Phys. Oceanogr., 49, 3221–3244, https://doi.org/10.1175/JPO-D-19-0083.1, 2019.

Rintoul, S., Hughes, C., and Olbers, D.: The Antarctic Circumpolar Current system, International Geophysics Series, 77, 271–302, 2001.

Roberts, M. J., Jung, T., Ortega, P., Ghosh, R., Wachsmann, F., von Storch, J.-S., Kroeger, J., Aengenheyster, M., & Roberts, C. D.: Phase 1 simulations, including HighResMIP and CMIP6- PI-control simulations. Zenodo. https://doi.org/10.5281/zenodo.14288726, 2024.

Spira, T., Swart, S., Giddy, I., and du Plessis, M.: The observed spatiotemporal variability of Antarctic Winter Water. J. Geophys. Res.: Oceans, 129, e2024JC021017. https://doi.org/10.1029/2024JC021017, 2024.